Science of the Total Environment 806 (2022) 150477

Contents lists available at ScienceDirect

Science of the Total Environment

journal homepage: www.elsevier.com/locate/scitotenv

Natural organic matter composition and nanomaterial *surface* coating determine the nature of platinum nanomaterial-natural organic matter corona

Mohammed Baalousha [a,*], Mithun Sikder [a], Brett A. Poulin [b,c], Malak M. Tfaily [d,e], Nancy J. Hess [d]

[a] South Carolina SmartState Center for Environmental Nanoscience and Risk (CENR), Department of Environmental Health Sciences, University of South Carolina, Columbia, SC 29208, USA
[b] U. S. Geological Survey, Boulder, CO 80303, USA
[c] Department of Environmental Toxicology, University of California Davis, Davis, CA 95616, USA
[d] Environmental Molecular Sciences Laboratory, Pacific Northwest National Laboratory, Richland, WA 99354, USA
[e] Department of Environmental Science, University of Arizona, AZ, USA 85721

HIGHLIGHTS

- Natural organic matter corona on PtNM surfaces (PtNM-NOM corona) was determined.
- PtNM-NOM corona composition varies with NOM composition and PtNM surface coating.
- The % of NOM formulas sorbed on PVP-PtNM was higher than those sorbed on cit-PtNM.
- PVP-PtNM NOM corona is richer than citrate-PtNM-NOM corona with condensed hydrocarbons.
- PtNM-NOM corona is rich with compounds with high molecular weight.

GRAPHICAL ABSTRACT

NM-NOM corona as a function of NM surface coating and NOM composition.

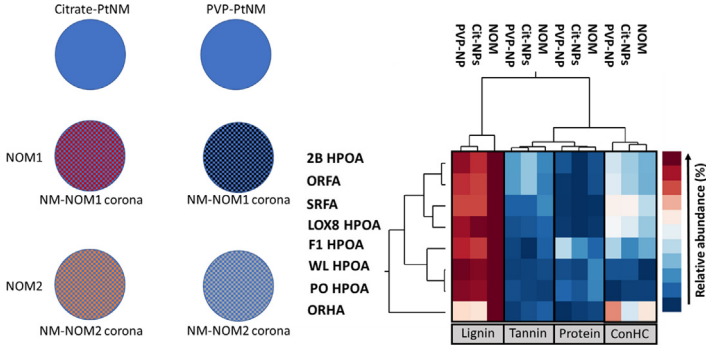

ARTICLE INFO

Article history:
Received 11 August 2021
Received in revised form 15 September 2021
Accepted 16 September 2021
Available online 20 September 2021

Editor: Damià Barceló

Keywords:
Natural organic matter
Corona
Platinum
Nanomaterials
Surface coating
Molecular properties

ABSTRACT

Natural organic matter corona (NOM corona) is an interfacial area between nanomaterials (NMs) and the surrounding environment, which gives rise to NMs' unique surface identity. While the importance of the formation of natural organic matter (NOM) corona on engineered nanomaterials (NMs) to NM behavior, fate, and toxicity has been well-established, the understanding of how NOM molecular properties affect NOM corona composition remains elusive due to the complexity and heterogeneity of NOM. This is further complicated by the variation of NOMs from different origins. Here we use eight NOM isolates of different molecular composition and ultrahigh resolution Fourier-transform ion cyclotron resonance-mass spectrometry (ESI-FT-ICR-MS) to determine the molecular composition of platinum NM-NOM corona as a function of NOM composition and NM surface coating. We observed that the composition of PtNM-NOM corona varied with the composition of the original NOM. The percentage of NOM formulas that formed PVP-PtNM-NOM corona was higher than those formed citrate-PtNM-NOM corona, due to increased sorption of NOM formulas, in particular condensed hydrocarbons, to the PVP coating. The relative abundance of heteroatom formulas (CHON, CHOS, and CHOP) was higher in the PVP-PtNM-NOM corona than in citrate-PtNM-corona which was in turn higher than those in the original NOM isolate, indicating preferential partitioning of heteroatom-rich molecules to NM surfaces. The relative abundance of CHO, CHON, CHOS, CHOP and condensed hydrocarbons in PtNM-NOM corona increased with their increase in NOM isolates. Furthermore, PtNM-NOM corona is rich with compounds with high molecular weight. This study demonstrates

* Corresponding author at: Department of Environmental Health Sciences, University of South Carolina, 921 Assembly Street, Columbia, SC 29208, USA.
E-mail address: mbaalous@mailbox.sc.edu (M. Baalousha).

https://doi.org/10.1016/j.scitotenv.2021.150477

that the composition and properties of PtNM-NOM corona depend on NOM molecular properties and PtNM surface coating. The results here provide evidence of molecular interactions between NOM and NMs, which are critical to understanding NM colloidal properties (*e.g.,* surface charge and stability), interaction forces (*e.g.,* van der Waals and hydrophobic), environmental behaviors (*e.g.*, aggregation, dissolution, sulfidation, *etc.*), and biological effects (*e.g.*, uptake, bioaccumulation, and toxicity).

1. Introduction

Nanomaterial-natural organic matter corona (NM-NOM corona) forms by the selective sorption of NOM molecules on nanomaterial surfaces. NM-NOM corona is thus the primary interface that determines NM surface identity, surface characteristics (*e.g.,* reactivity, adsorption capacity, charge), environmental behavior (*e.g.,* aggregation, (Ghosh et al., 2011; Loosli et al., 2013; Mohd Omar et al., 2014) dissolution, (Baalousha et al., 2015; Gunsolus et al., 2015; Linlin and Tanaka, 2014) and sulfidation (Zhang et al., 2016)), and biological interactions (*e.g.,* bioavailability and toxicity) (Kteeba et al., 2017). For instance, higher molecular weight NOM increases the stability of AuNMs due to increased electrosteric repulsion. (Louie et al., 2015; Louie et al., 2013; Nason et al., 2012a) Additionally, aggregation of ZnS particles (laboratory simulation of natural ZnS particles) decreased with increasing NOM concentration, molecular weight, and aromatic content of NOM fractions (Deonarine et al., 2011b). On the other hand, Pony Lake fulvic acid (PLFA) mitigated AgNM toxicity to the nematode *Caenorhabditis elegans* more effectively than SRFA (Ücer et al., 2006), which was attributed to the higher metal binding capacity of PLFA compared to SRFA due to compositional differences between these two NOMs. PLFA has higher N and S contents (6.5% N, 3.0% S) than SRFA (0.72% N, 0.44% S), suggesting that PLFA has a higher percentage of amine ligands and reduced sulfur groups that provide more binding sites for Ag^{+} and AgNM surfaces (Afshinnia et al., 2016; Gondikas et al., 2012). Tannic acid has also been shown to reduce ZnO toxicity more efficiently than fulvic acid and humic acid by reducing bioavailability of free Zn^{2+} in aqueous media (Yang et al., 2013). In addition, compared to NOM samples, proteins and carbohydrates were less effective in mitigating ZnO-NMs toxicity in embryonic zebrafish (Kteeba et al., 2017).

Several studies demonstrated the formation of NOM corona on NM surfaces using various analytical techniques. For instance, using field flow fractionation to measure the increase in the NM hydrodynamic diameter, Suwannee River humic acid (SRHA) was shown to form a < 1 nm thick surface layer around 7 nm iron oxide NMs, and the thickness of this layer increased with the increase in SRHA concentration (Baalousha, 2009; Baalousha et al., 2008). Another study demonstrated, using high resolution transmission electron microscopy-coupled with electron energy loss spectrometry, that SRFA form a 1.3 nm oxygen-containing corona around 20 nm citrate coated AgNMs (Römer et al., 2016). Additionally, spectroscopic evidence identified strong sorptive fractionation that occurs between diverse organic compounds of humic substances and NM surfaces (Claret et al., 2008; Ghosh et al., 2009; Meier et al., 1999). In addition, the hydrophobic fraction of fulvic acids (and/or the organic molecules with high contents in aromatic moieties rich with oxygen containing functional groups) were preferentially sorbed compared to aliphatic fractions on metallic oxide mineral surfaces (Claret et al., 2008; Kaiser, 2003; Meier et al., 1999). Moreover, size-exclusion-chromatography and spectroscopic analysis of fulvic or humic acids highlight the fractionation of molecules based on size during adsorption to mineral surfaces (Hur and Schlautman, 2004), which was attributed to structural trends in the molecular weight fractions (*e.g.,* degree of aromaticity, chemical functionality and the underlying adsorption processes). Selective adsorption of high molecular weight (HMW) compounds, aromatic, hydrophobic compounds on the surfaces of natural and engineered NMs has been reported through bulk measurement techniques (*i.e.,* fractionation and UV–Vis) (Avneri-Katz et al., 2017). However, few studies describe the molecular level composition and properties of NOM molecules that selectively sorb on the surface of NMs and form NM NOM-corona.

NOM is a complex mixture of polyelectrolytic and polyfunctional organic molecules (*tens of thousands of unique chemical species*) that vary spatially and temporally in molecular composition, acidity, molecular weight and structure, and charge density (Gu et al., 1994). Ultrahigh resolution-Fourier transform-ion cyclotron resonance-mass spectrometry (FT-ICR-MS) offers resolving power sufficient for identification of NOM compounds at the level of elemental composition assignment. FT-ICR-MS is a technique that measures the mass-to-charge ratio of organic compounds with up to six decimal place precision (D'Andrilli et al., 2010). Thus, FT-ICR-MS provides elemental composition assignment for compounds with the same nominal mass-to-charge ratio (m/z), but differing in exact mass, critical to elucidate NOM and selective adsorption to NMs. Recently, FT-ICR-MS was used to quantify that AgNM-NOM corona is rich with N- and S-containing compounds, compounds with high molecular weight, high unsaturation, and high number of oxygenated groups (Baalousha et al., 2018). Other studies, using FT-ICR-MS, showed the enrichment of highly reactive, acidic, oxygen functionalized aromatic and aliphatic molecules on alumina surfaces (Galindo and Del Nero, 2014; Galindo and Del Nero, 2015). Another study demonstrated that ferrihydrite exhibits higher affinity to NOM than does goethite or lepidocrocite, and HMW (>500 Da) compounds and compounds high in unsaturation or rich in oxygen (including polycyclic aromatics, polyphenols and carboxylic compounds) had higher affinity to iron oxyhydroxides, and especially ferrihydrite (Lv et al., 2016).

Most studies investigating NOM-NM interactions use a limited number of NOM isolates (typically humic substances provided by the International Humic Substances Society), hampering the understanding of how NOM molecular composition determines the nature of NM-NOM corona. Here, we characterize NOM corona formed on the surface of citrate- and polyvinylpyrrolidone-coated PtNMs (cit- and PVP- PtNMs) platinum at the molecular level through negative-ion electrospray ionization FT-ICR-MS. The molecular compositions of the eight NOM samples reflect diverse source material. Platinum has been used in vehicle catalytic convertors to oxidize carbon monoxide to hydrocarbons for several decades, which has resulted in increased release, and thus concentrations, of platinum in the environment (Bocca et al., 2003; Morton et al., 2001; Schäfer and Puchelt, 1998). A recent study demonstrated Pt NM release from catalytic convertors (Folens et al., 2018). To better predict the environmental concerns regarding the potential environmental implications (*e.g.*, bioaccumulation and/or toxicity) of PtNMs (Pawlak et al., 2014), this study quantified at the molecular level the selective sorption of NOM from diverse aquatic systems.

2. Materials and methods

2.1. Preparation of PtNMs

Citrate- and polyvinylpyrrolidone-coated PtNMs (cit-$PtNM_{75}$ and PVP-$PtNM_{75}$, where 75 denote particle core size measured by TEM in nm) were synthesized using a seed-mediated growth method according to the protocol presented elsewhere (Sikder et al., 2019). Briefly, spherical cit-PtNM seed suspensions (8.7 nm diameter) were synthesized by adding 36 mL of 5 mM chloroplatinic acid hydrate (H_2PtCl_6, ≥ 99.9% pure, supplied by Sigma-Aldrich, St. Louis, USA) to 464 mL ultra-high

pure water (UHPW, 18.2 MΩ· cm) at the boiling point in a 1000 mL Erlenmeyer flask, followed by adding 50 μL of 1 M sodium hydroxide (NaOH, supplied by Sigma-Aldrich, St. Louis, USA) and 11 mL of 38 mM sodium citrate solution. After 30 s, 5.5 mL of a solution containing 21 mM sodium borohydride ($NaBH_4$, > 98% pure, supplied by Alfa Aesar, Ward Hill, USA) and 1% sodium citrate ($Na_3C_6H_5O_7$, supplied by VWR International, West Chester, USA) were added quickly to the boiling solution. After 10 min of boiling, the product was left to cool to room temperature. All reactions took place under vigorous stirring (*i.e.,* 700 rpm). cit-$PtNM_{75}$ were synthesized by diluting 2.5 mL of the seed PtNM suspension in 298 mL UHPW, to which 450 μL of 0.4 M H_2PtCl_6 were added under constant stirring (700 rpm). 5 mL solution containing 1% sodium citrate and 1.25% L-ascorbic acid were then added dropwise (1 drop per 3 s). The temperature was increased slowly to 100 °C with an increment of 10 °C per minute under vigorous stirring for 30 min and then left to cool to room temperature. The cit-$PtNM_{75}$ suspension was washed three times by ultrafiltration to remove excess reagents. 300 mL cit-$PtNM_{75}$ suspension were reduced to 150 mL by ultrafiltration over 3 kDa regenerated cellulose membrane using an Amicon® stirred-cell ultrafiltration unit (EMD Millipore Corporation, MA, USA) under 105 kPa (nitrogen). The PtNM suspension was replenished with 150 mL solution of 1% sodium citrate. PVP-$PtNM_{75}$ were obtained by a ligand exchange approach using cit-$PtNM_{75}$ as precursors (Tejamaya et al., 2012). Briefly, 300 mL cit-$PtNM_{75}$ were converted into PVP-$PtNM_{75}$ by adding 0.12 mL of 7.7 mM PVP solution under vigorous stirring (700 rpm) for at least 1 h. The PVP amount selected was that required to obtain a surface coverage of PtNMs by 8 PVP molecules nm^{-2} (Afshinnia et al., 2017). Citrate and PVP surface coatings were used as model surface coatings because they are well-characterized, widely used in published studies, impart two mechanisms of NM stabilization (*e.g.,* electrostatic stabilization and steric stabilization, respectively) (Afshinnia et al., 2017; Baalousha, 2017), and they are likely to interact in dissimilar ways with NOM.

The concentrations of synthesized cit- and PVP-PtNMs were measured using a NexION 350D inductively coupled plasma-mass spectrometer (ICP-MS). One mL aliquots of each PtNM suspension were digested using 1 mL freshly-prepared aqua regia at room temperature for 24 h. Aqua regia was prepared by mixing 1 mL hydrochloric acid (trace metal grade, 35–38%, Fisher scientific, MA, USA) and 3 mL nitric acid (trace metal grade, 68–70%, Fisher scientific, MA, USA) in acid cleaned glassware. The digested PtNM solutions were diluted at least 3000 folds prior to analysis by ICP-MS, and all samples were measured in triplicate.

2.2. NOM sampling sites and sample collection

The hydrophobic acid (HPOA) fraction of NOM was isolated from a wide range of aquatic environments including: three saw-grass dominated wetlands in the northern Florida Everglades Water Conservation Area (WCA) 2A at site F1 (F1 HPOA), WCA 2B (2B HPOA), and Arthur R. Marshall Loxahatchee National Wildlife Refuge (LOX) at site 8 (LOX8 HPOA); Williams lake (Minnesota; WL HPOA); Pacific Ocean surface water near Hawaii (PO HPOA); the Suwannee River (Georgia; SRFA); Ogeechee River humic acid (Georgia; ORHA); and Ogeechee River fulvic acid (Georgia; ORFA). The HPOA fraction of NOM was isolated on XAD-8 resin (Aiken et al., 1992), which is a chemically distinct NOM fraction that is recognized as reactive to engineered NPs (Jiang et al., 2017). For two of the samples, the HPOA fraction was further separated into humic acid and fulvic acid fractions (precipitation at pH 1). NOM samples were freeze-dried immediately after isolation to minimize NOM alternation prior to NM-NOM interaction experiments. Additional details on the isolation of the Everglades (Poulin et al., 2017) and Pacific Ocean samples (Green et al., 2014) are available elsewhere. The NOM isolates were characterized by determining their elemental composition using a CHONS analyzer and specific ultraviolet light absorbance at 254 nm ($SUVA_{254}$) using UV–vis spectrometer as described elsewhere (Huffman and Stuber, 1985; Weishaar et al., 2003). The properties of the eight NOMs used in this study are presented in Table S1.

2.3. Formation and isolation of PtNM-NOM corona

Eight NOM samples, isolated from different environments, were compared to highlight compositional differences between NOM corona formed by selective adsorption of NOM molecules on the surface of cit- and PVP- PtNMs. Stock solutions of NOM samples (50 mg L^{-1}) were prepared by dissolving 1 mg of freeze-dried NOM in 20 mL ultrapure water. The pH was adjusted to 7.0 through addition of 0.1 or 1 M NaOH. Aliquots of NOM and cit- or PVP- PtNM stock suspension were added to UHPW to yield a final volume of 45 mL of a final NOM concentration of 4 mg L^{-1} and PtNM concentration of 2 mg-Pt L^{-1}. NOM and NOM-PtNM mixtures were left for 24 h to equilibrate. The NOM and NOM-PtNM samples were then centrifuged at 16,000 rpm for 1 h (Thermo Scientific) to remove PtNMs and the top 15–20 mL were transferred to 50 mL centrifuge tubes (Corning™ Falcon). The decanted NOM samples were acidified to pH 2 with H_3PO_4, extracted by Solid-Phase Extraction (SPE) on PPL (modified styrene divinyl benzene polymer type sorbents, Agilent Tech, USA) cartridges, and eluted with HPLC-grade methanol to concentrate NOM and remove salts (Dittmar et al., 2008; Tfaily et al., 2012). All experiments were performed in triplicates. Formulas forming NOM corona were identified as those present in at least two of the three NOM replicates and absent in two of the corresponding three NOM-PtNM supernatant replicates. Formulas in common in Cit-PtNM-NOM corona and PVP-PtNM-NOM corona are those present in Cit-PtNM-NOM corona and PVP-PtNM-NOM corona. Formulas unique to Cit-PtNM-NOM corona are those present in Cit-PtNM-NOM corona and absent in PVP-PtNM-NOM corona, and *vice versa*.

2.4. EST-FT-ICR-MS analysis

A 12 Tesla Bruker Solarix FT-ICR-MS located at the Environmental Molecular Sciences Laboratory in Richland, WA, was used to collect high-resolution mass spectra of the NOM isolates. A standard Bruker ESI source was used to generate negatively charged molecular ions. Samples were introduced directly to the ESI source at a flow rate of 3 μl min^{-1} (Orton et al., 2018). The ion accumulation time was 0.05 s, to account for differences in C concentration between samples and to maintain a final dissolved organic carbon (DOC) concentration of 20 mg L^{-1}. The instrument was externally calibrated weekly with a tuning solution from Agilent (Santa Clara, CA), which calibrates to a mass accuracy of <0.1 ppm. Three hundred scans were averaged for each sample and internally calibrated using OM homologous series separated by 14 Da ($-CH_2$ groups). The mass measurement accuracy was less than 1 ppm for singly charged ions across a broad *m/z* range (*i.e.* 200 < m/z ⟨1200) and the analytical reproducibility of the instrument ranged between 85 and 90% based on Suwannee River Fulvic Acid standard (SRFA), obtained from the International Humic Substances Society (IHSS). Further, for each sample, three analytical replicates were analyzed, and reproducibility of the instrument was further calculated based on the total number of common and unique peaks among the three replicates, which was >85% for all samples. Thus, data analysis proceeded by including peaks that were present in two out of three replicates for each sample. To further reduce cumulative errors, all sample peak lists for the entire dataset were aligned to each other prior to formula assignment to eliminate possible mass shifts that would impact formula assignment. Putative chemical formulas were assigned using Formularity software (Tfaily et al., 2015; Tolic et al., 2017). Chemical formulas were assigned based on the following criteria: S/N > 7, and mass measurement error < 1 ppm, taking into consideration the presence of C, H, O, N, S and P and excluding other elements. Peaks with large mass ratios (*m/z* values >500 Da) were assigned formulas through the detection of homologous series (CH_2, O, H_2). Additionally, to ensure consistent assignment of molecular

formulas the following rules were implemented: (1) one phosphorus requires at least four oxygens in a formula, (2) N<=3 and S<3, and (3) when multiple formula candidates were assigned, the formula with the lowest error and with the lowest number of heteroatoms was picked. The molecular formulas were grouped into seven heteroatom classes: CHO, CHON, CHOS, CHOP, CHONS, CHONP, and CHONSP. Further, the molecular formulas were grouped into right tentative chemical compound classes according to Tfaily et al. (2015) including: condensed aromatic compounds, unsaturated hydrocarbons, tannins, lignin/carboxyl-rich alicyclic molecules (CRAM), lipids, proteins, amino sugars, and carbohydrates derived. It is important to note that CRAM fits within the van Krevelen space labeled "lignin-like". Assignments of molecular formulas to compound classes are tentative because structural information cannot be gained from molecular stoichiometries alone. Additional analysis is required to tease apart whether lignin and/or CRAM exist in the samples. As such, we included both identifications in the discussion. From the formula assignment, the relative (by number-weighted) abundance of each heteratom and compound class was calculated and compared between NOMs and NOM-coronas (Tfaily et al., 2015).

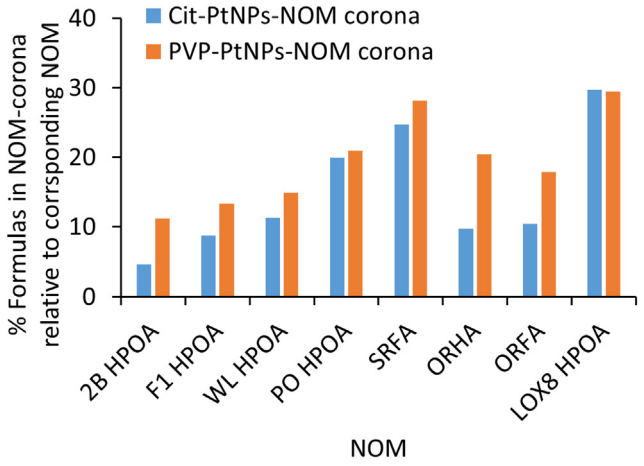

Fig. 1. Percentage of NOM formulas that make up PtNM-NOM corona relative to the number of molecules in the corresponding NOM sample.

2.5. Statistical analysis

Principal component analysis (PCA) and cluster analysis by JMP Pro15 were used to assess differences in the elemental composition between the different samples using the relative abundance of the different compound classes identified by FTICR-MS, in particular lignin-like/CRAM, protein-like, tannin-like, and condensed hydrocarbon compounds. The latter was calculated using a distance matrix between the samples using the Bray−Curtis distance measure. Ward's linkage method was used to group the samples, and the cluster analysis results were presented as a dendrogram and a constellation plot. The Constellation Plot was used to show the membership in clusters as they're built up from the cluster analysis (*i.e.,* to show the structure of the tree). The axis here are just for scaling and don't have any relevance. The circle in the middle is used to identify the root of the tree. Correlation coefficients between heteroatom classes and compound classes in NOM and those forming NOM-coronas were calculated using Pearson's correlation method and the *p*-value for correlation was calculated using *t*-test. In all cases, the statistical significance was set at *p*-value <0.05.

3. Results and discussion

3.1. Molecular properties of NOMs and PtNMs-NOM corona

Elemental composition derived from FT-ICR-MS spectra can be rapidly visualized in Van Krevelen diagrams, which plot H/C *vs.* O/C ratios. Fig. S1 shows the van Krevelen diagram for the identified formulas in NOMs, citrate-PtNM NOM corona, PVP-PtNM NOM corona, common to citrate and PVP-PtNM NOM corona, and those unique in citrate- or PVP-PtNM NOM coron. Fig. S1 illustrates qualitatively the overall differences in the molecular composition and properties of NOMs and NOM coronas formed on citrate and PVP-PtNMs (Fig. S1). It also illustrates the selective sorption of NOM formulas on the surfaces of PtNMs. These differences are discussed quantitively below.

Approximately 5 to 30% of all molecules in NOMs partitioned to NM surfaces to form PtNM-NOM corona (Fig. 1). The relative abundance of NOM formulas that formed the PVP-PtNMs-NOM corona are modestly higher compared to those that formed the cit-PtNMs-NOM corona (Fig. 1). This is likely due to the differences in the nature of NOM interaction with cit- and PVP- coated PtNMs. Citrate interacts with NM surfaces through the oxygen atom in the carboxylate groups of the citrate molecule (Frost et al., 2017). Citrate is weakly associated with the NM surfaces and is readily displaced by a range of other molecules including thiols, amines, polymers, and proteins (Perera et al., 2018). On the other hand, PVP is a polymer that binds strongly to NM surface, and is more difficult to displace. PVP forms covalent bonds between the pyrrolidone subunits and the surface of PtNMs (Kan et al., 2005; Zhang et al., 2008). The interactions form through electron donation from either nitrogen (M-N coordination) (Khanna et al., 2004; Koczkur et al., 2015), or oxygen (M-O coordination) (Gao et al., 2004; Henglein, 1998) on a pyrrolidone subunit to the metal surfaces. The more dominant interaction is between the carbonyl of the PVP and the surfaces of noble metal NMs (Kedia and Kumar, 2012).

The chemistry of NM surfaces can exhibit dynamic changes in response to the local environment. Citrate can be readily displaced from NM surfaces by organosulfur such as organothiols (R-SH), organodisulfide (R-S-S-R), and non-specific ligands including halides and adenine (Perera et al., 2018). Additionally, NOM (fulvic and humic acids) can readily displace the citrate coating on the surface of NMs (*e.g.,* Au and Ag) (Diegoli et al., 2008; Lau et al., 2013), and that carboxyl and hydroxyl groups interact with the surfaces of NMs (*e.g.,* Ag) (Lau et al., 2013). Thus, we hypothesize that NOM displaces citrate from the surface of cit-PtNMs and interacts directly with cit-PtNM surfaces. On the other hand, the interaction of NOM with PVP-PtNMs is likely due to the interaction of NOM with the PVP-coating itself, and/or due to diffusion of NOM molecules through PVP coating toward PtNM surfaces. It has been shown that NOM interacts with both the ring and polyvinyl domains of PVP, that the oxygen atom is involved in the PVP-AgNM complex, and that hydrophobic/steric forces play an important role in the adsorption of NOM on PVP-AgNMs (Lau et al., 2013). Additionally, the PVP-PtNPs used in this study are partially coated with PVP and citrate (Sikder et al., 2019) allowing direct interaction between PtNM and heteroatom classes of compounds as for cit-PtNMs.

CHO molecules are the dominant formulas that make up the NOM samples and the PtNM-NOM corona, representing *ca.* 40–80% of all formulas (Fig. 2a). However, CHON, CHOS, and CHOP molecules represent a significant fraction of NOM formulas forming NOM corona (Fig. 2b-d), demonstrating the important role of heteroatoms in determining the elemental composition of NOM corona. The relative abundance of CHO formulas in NOM corona is lower compared to the relative abundance of CHO formulas in the corresponding NOM and decreases following the order NOM > PVP-PtNMs-NOM corona ~ > cit-PtNMs-NOM corona. The relative abundance of CHON and CHOS formulas is typically higher in NOM-corona compared to the corresponding NOM (Fig. 2b and c). CHOP formulas were higher in NOM corona for some NOMs and lower for other NOMs. Additionally, the relative abundance of CHOP formulas in formulas unique to cit-PtNPM corona was higher than those in the unique formulas PVP-PtNOM corona (Fig. 2d), likely due to the direct interaction of NOM molecules with the surface of PtNMs in the case of cit-PtNMs. These results indicates the selective sorption of CHON and CHOS formulas compared to CHO and CHOP formulas, interpreted to be the result of the higher affinity of compounds

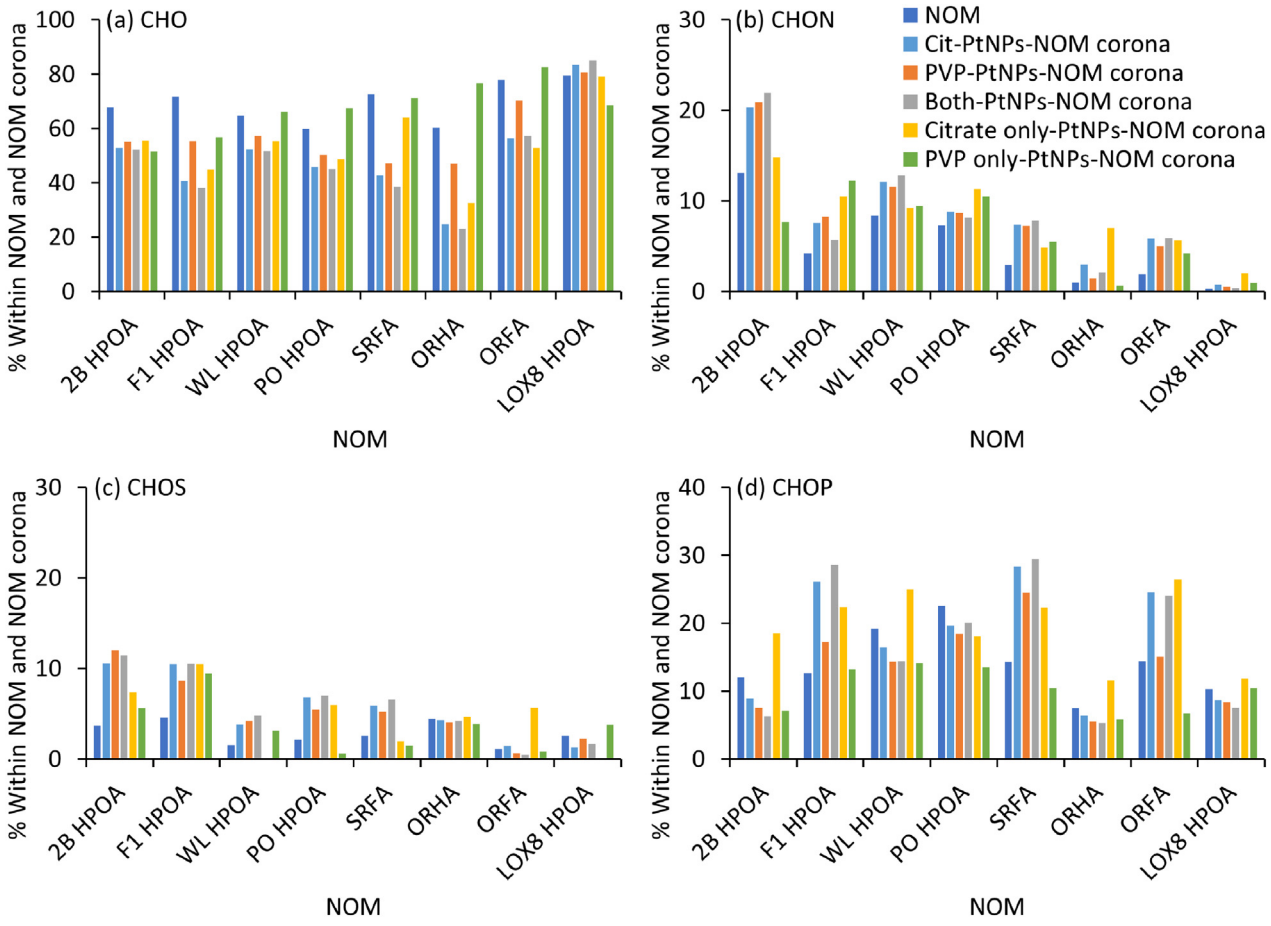

Fig. 2. Percentage of compound classes grouped by heteroatom that make up NOM and PtNMs-NOM corona: (a) CHO, (b) CHON, (C) CHOS, and (d) CHOP. Both refers to common formulas in cit-PtNM-NOM corona and PVP-PtNM-NOM corona. Citrate only refers to formulas present in citrate NOM corona and absent in PVP-PtNM-NOM corona. PVP only refers to formulas present in PVP-PtNM-NOM cotona and absent in cit-PtNM-NOM corona.

with S and N functional groups to NM surfaces (Hu et al., 2016) compared to CHO compounds (*e.g.,* O containing functional groups).

The binding of organic molecules to PtNM surfaces depends strongly on the functional groups (Wand et al., 2016). Pt and Ag are soft metals and are likely to react with the same ligands *e.g.,* soft bases (*e.g.,* P and S containing functional groups) forming covalent bonds, as well as with O containing functional groups. Nobel metal NM surfaces interact with O-alkyle groups in NOM, such as those found in sugars, polysaccharides, and ether lipids (Lau et al., 2013). Reduced sulfur containing functional groups (*e.g.,* thiol) form strong covalent bond with PtNM *via* the sulfur atoms (Wand et al., 2016). On the other hand, amine functional groups bind to PtNM surfaces *via* electrostatic interactions, H-bond, or the lone-pair of the nitrogen (Ryu et al., 2011). In charged systems under acidic conditions, the ligand may mainly bind *via* electrostatic interactions to NM surfaces. In this mode, the positively charged ammonium cations interact with negative charges at the NM surfaces and form relatively strong bonds (Fink et al., 1998; Özkar and Finke, 2002; Thomas et al., 2002). In a strong basic environment (*e.g.,* pH > 10), because of the absence of protonated species, amine binds *via* the lone-pair of the nitrogen atom to the particles (Ryu et al., 2011).

Based on compound classes, organic matter chemical composition was clearly different between the eight NOM samples, as inferred from PCA (Fig. 3a) and cluster analysis plots (Fig. 3b) and appear to be shaped in part by the abundance of four compound classes: lignin-like, protein-like, tannin-like, and condensed hydrocarbon-like compounds (Fig. 3b). For example, the relative abundance of lignin decreased in all NOM samples due to sorption to PVP-PtNM and cit-PtNM surfaces. This was evident by the fact that i) the loading vector for lignin/CRAM was correlated with free NOM; ii) the two-way cluster analysis revealed a decrease in the abundance of lignin-like compounds in the presence of nanoparticles; and iii) the cluster that represents lignin-like compounds within the constellation plot (Fig. 3C) showed that the node representative of NOM alone was separate from the nodes that represent PVP-PtNPs and Cit-PtNPs. Further, the initial differences in organic matter composition between these eight NOMs drove the differences between PVP-PtNPs and Cit-PtNPs for a given NOM and among different NOMs. Four clusters were identified in the constellation plots based on four main compound classes. Within each cluster, clear separation was observed in NOM composition due to treatment.

Most NOM molecules that make up the NOM and NOM corona are lignin/CRAM followed by condensed hydrocarbons, tannins, and protein (Fig. 4). Other classes of compounds represent <3% of the overall NOM and NOM corona and thus are not discussed here. The abundance of lignin/CRAM in PtNM-NOM corona was generally smaller than that in the NOM (Fig. 4a), but still represented most NOM formulas in PtNM-NOM corona due to their high abundance in NOM samples. The relative abundance of lignin/CRAM in PVP-PtNM-NOM corona was slightly higher than the relative abundance of lignin/CRAM in cit-PtNMs-NOM corona, which may be attributed to the higher hydrophobicity of PVP relative to citrate (Song et al., 2011). Lignin/CRAM have hydrophilic regions (*e.g.,* hydroxyls (–OH), carboxylic (–COOH) and small alkyl chains and hydrophobic regions (*e.g.,* resinol, C—H groups). These hydrophilic and hydrophobic regions enable lignin/CRAM to bind with particle surfaces through polar, covalent, and hydrogen bonding as well as Van der Waals forces. The PtNM-NOM corona is generally enriched by condensed hydrocarbons compared to the corresponding NOM (Fig. 4b). In general, the relative abundance of condensed hydrocarbons was higher in PVP-PtNMs-NOM corona compared to Cit-PtNMs-NOM corona, which may

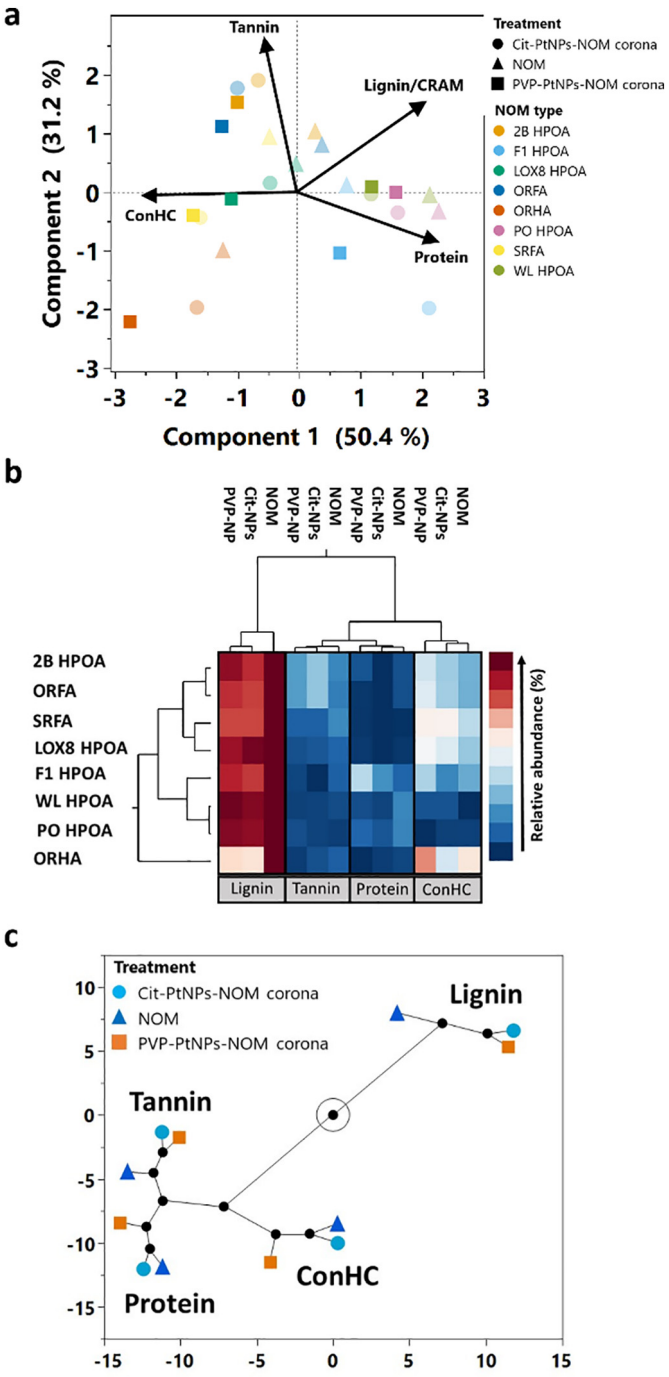

Fig. 3. (A) A PCA plot of the first twos PCs. The explained variances are shown in brackets; (B) Hierarchical cluster dendrogram of the molecular composition from all NOM samples under different treatments (initial NOM, PVP-PtNM, and Cit-PtNM); (C) Cluster constellation plot illustrating the number of clusters in which the centroids are clusters are embedded in the plane of panel C and the cross-sample relationships are plotted as lines connecting related sample clusters (clades). Four clusters were identified based on four main compound classes. Within each cluster, clear separation was observed in NOM composition due to treatment (initial NOM, PVP-PtNM, and Cit-PtNM).

be attributed to the higher hydrophobicity of PVP relative to citrate[67]. The relative abundance of condensed hydrocarbons in molecules common to both Cit-PtNM- and PVP-PtNM-NOM coronas was lower than the relative abundance of condensed hydrocarbons in some NOMs (*e.g.,* F1 HPOA, PO HPOA, ORHA) and higher in other NOMs (*e.g.,* 2B HPOA, WL HPOA, SRFA, ORFA, and LOX8 HPOA). More interestingly, the relative abundance of condensed hydrocarbons was higher in the molecules unique to PVP-PtNM-NOM corona than in the molecules unique to cit-PtNM-NOM corona. This is consistent with the chemical structure of PVP and citrate. PVP is uncharged with an amide group that favors dissolution. However, the polymer backbone has significant hydrophobic moieties (six carbon per monomer unit) (Song et al., 2011). Conversely, citrate is a small molecular weight carboxylic acid that is very hydrophilic and miscible in water. Nonpolar organic materials with low aqueous solubility can have stronger attractions to hydrophobic surfaces in aqueous environments through hydrophobic interaction (Hummer et al., 1996; Lazaridis and Paulaitis, 1992). Tannin-like molecules did not show clear trend in partitioning to PtNM surfaces, exhibited both higher and lower abundance of tannins compared to their relative abundance in the corresponding NOM

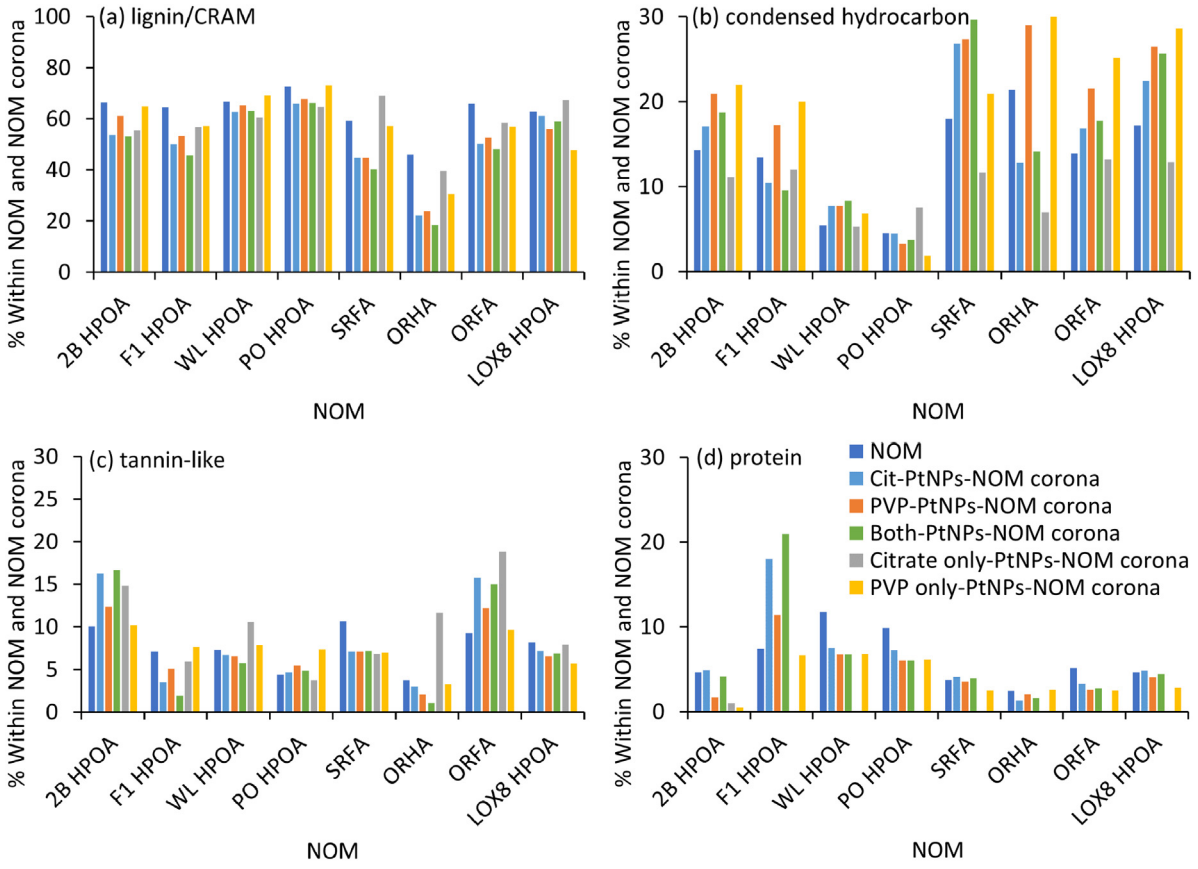

Fig. 4. Percentage of NOM formulas that make up initial NOM and Pt-NM-NOM corona by compound class: (a) Lignin/CRAM-like, (b) condensed hydrocarbon-like, (c) tannin-like, and (d) protein-like.

(Fig. 4c). Except for F1 HPOA, PtNMs-NOM corona exhibited lower relative abundance of protein compared to relative abundance of protein in NOMs (Fig. 4d).

The molecular weight of NOM formulas forming PtNM-NOM corona are higher than the molecular weight of the corresponding NOM formulas (Fig. 5). This agrees with previous studies demonstrating the selective adsorption of higher molecular weight compounds on NMs or mineral surfaces (Davis and Gloor, 1981; Lv et al., 2016; Mwaanga et al., 2014; Zhou et al., 2001). For instance, the molecular weight of NOM formulas forming AgNMs-NOM-corona was higher than the corresponding NOM indicating the selective sorption of high molecular weight formulas on AgNM surfaces (Baalousha et al., 2018). Additionally, Galindo and Del Nero (2014) demonstrated the selective adsorption of fulvic acid formulas with m/z values ranging from 120 to 980, with almost all fulvic acid formulas with m/z ≥ 775 selectively sorbing to the surface of aluminum oxide (Galindo and Del Nero, 2014). The increase in NOM corona molecular weight relative to NOM is consistent with the increase in the relative abundance of condensed hydrocarbons in NOM corona. This is because the higher MW NOM tends to have more aromatic carbon over aliphatic carbon moieties (Chin et al., 1994). The selective sorption of high MW NOM formulas and formulas rich with aromatic carbon have been shown to enhance the stability of PtNMs

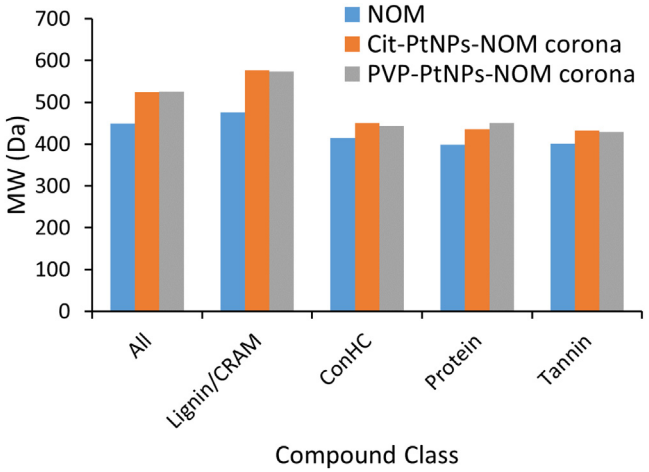

Fig. 5. The average MW of NOM and NOM-corona illustrated for PO HPOA.

Table 1
Pearson correlation between the properties of NOM-corona and those of the corresponding NOM. Significant correlation is indicated by the bold font.

Heteroatom/compound classes		R^2	*P-value*
CHON in NOM *vs* CHON in NOM-corona	Cit-PtNP	**0.94**	**0.0001**
	PVP-PtNP	**0.93**	**0.0001**
CHO in NOM *vs* CHO in NOM-corona	Cit-PtNP	0.47	0.0593
	PVP-PtNP	**0.59**	**0.0261**
CHOS in NOM *vs* CHOS in NOM-corona	Cit-PtNP	0.38	0.1052
	PVP-PtNP	0.36	0.1136
CHOP in NOM *vs* CHOP in NOM-corona	Cit-PtNP	0.20	0.2684
	PVP-PtNP	0.36	0.1177
ConHC in NOM *vs* ConHC in NOM-corona	Cit-PtNP	**0.51**	**0.0475**
	PVP-PtNP	**0.97**	**0.00001**
$SUVA_{254}$ *vs.* ConHC in NOM-corona	Cit-PtNP	0.33	0.1339
	PVP-PtNP	**0.84**	**0.0013**
Lignin/CRAM in NOM *vs* Lignin/CRAM in NOM-corona	Cit-PtNP	**0.85**	**0.0010**
	PVP-PtNP	**0.93**	**0.0001**
Tannin in NOM *vs* Tannin in NOM-corona	Cit-PtNP	0.47	0.0608
	PVP-PtNP	**0.57**	**0.0295**

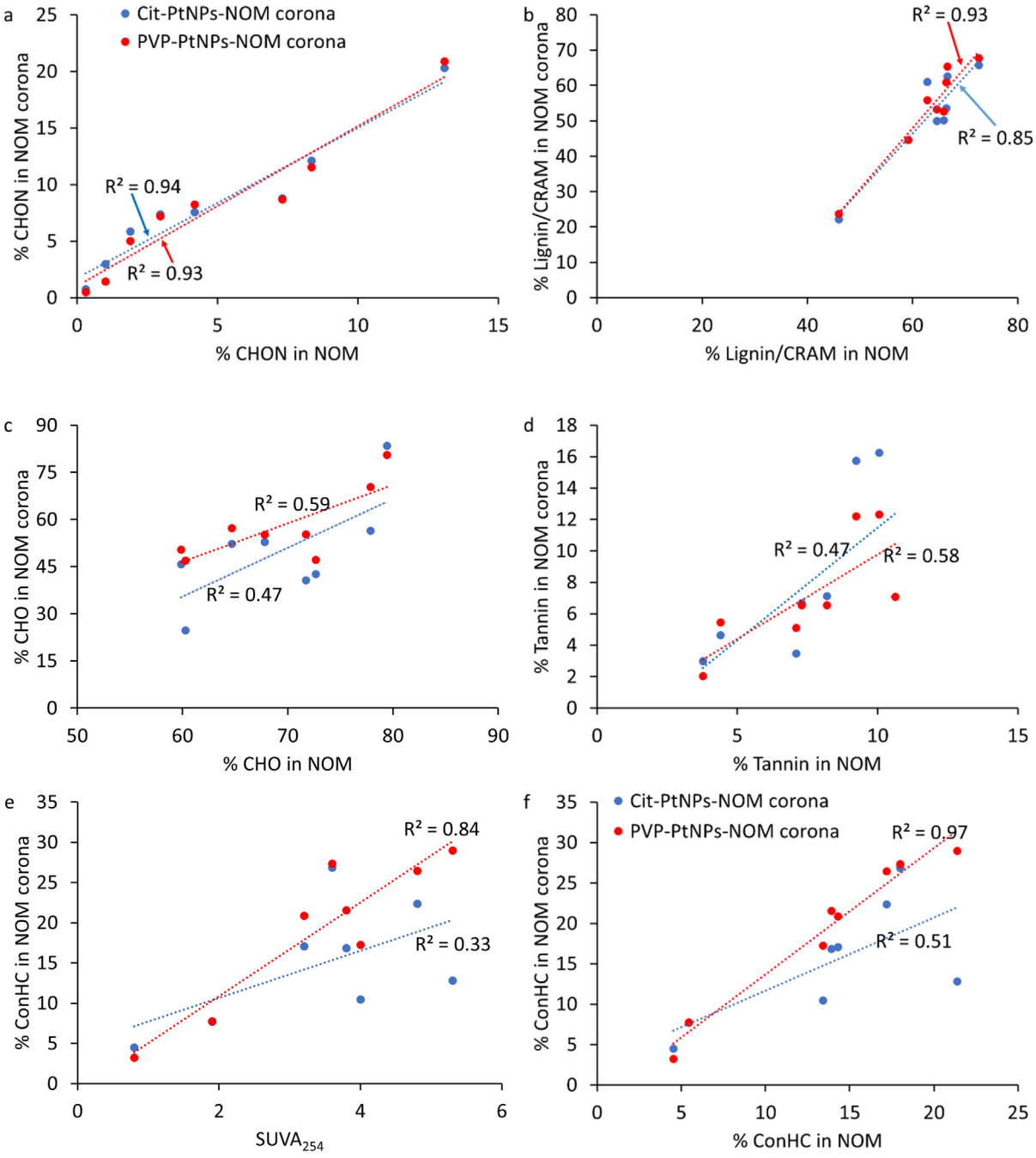

Fig. 6. Correlation between the percentage number of formulas in NOM and the corresponding cit- and PVP-PtNMs-NOM corona (a) CHON and (b) lignin/CRAM, (c) CHO, (d) Tannin, (e) $SUVA_{254}$, and (f) ConHC.

(Sikder et al., 2020), ZnS NMs (Deonarine et al., 2011a), and cit-AuNMs (Nason et al., 2012b).

3.2. Correlation between NOM properties and PtNM-NOM properties

The NOM samples used in this study represents a diverse array of NOM compositional differences relevant to all aquatic systems. Differences in NOM composition among samples may explain the variation in the observed PtNM-NOM corona composition. To identify the NOM properties with the greatest influence on PtNM-corona composition, we performed Pearson's correlation analysis between NOM-corona properties and the corresponding NOM properties. Calculated Pearson's correlation coefficient (r) and *p-values* (Table 1) were used to assess the correlation quality with each NOM parameter.

NOM properties producing the best positive correlations with the NOM-corona properties for both cit-PtNMs and PVP-PtNMs were the relative abundance of CHON (R^2 = 0.93–0.94, *p*-value =0.0001, Fig. 6a) and the relative abundance of lignin/CRAM (R^2 = 0.85–0.93, *p*-value = 0.001–0.0013, Fig. 6b). Other NOM properties produced positive correlation for PVP-PtNMs only (*e.g.,* relative abundance of CHO, Tannin, and $SAUVA_{254}$, Fig. 6 bc-e) or produced higher positive correlation for PVP-PtNMs than Cit-PtNM-NOM (*e.g.,* relative abundance of condensed hydrocarbons, Fig. 6f). These more significant correlations with PVP than with citrate can be attributed to the higher hydrophobicity of PVP coating compared to citrate coating. Overall, these results illustrate that importance of the properties of NOM and NM surface coating in determining the composition of NOM corona.

4. Conclusions

Although it is well established that NOM sorb on the surfaces if NMs forming NM-NOM corona, factors affecting the composition of NM-NOM corona remain poorly understood. Some studies focused on selective adsorption of NOM on the surface of NMs using bulk analysis techniques. However, very few studies have focused on molecular level characterization of NOM corona. Using ESI-FT-ICR-MS, our results indicate that NOM corona composition is a function of NOM chemical composition and PtNM surface coating. Specifically, PtNM NOM corona is enriched with N- and S-containing formulas, condensed hydrocarbons, and formulas with HMW compared to the corresponding NOM from which NOM-corona formed. Additionally, PVP-PtNM-NOM corona is enriched with condensed hydrocarbon-like molecules relative to cit-PtNM-NOM corona. The findings of this study are critical to improve the understanding of the impact of NOM properties on the colloidal properties (*e.g.,* surface charge property), interaction forces between particles (*e.g.,* calculations of van der Waals and hydrophobic interactions), interaction with contaminants (*e.g.,* determination of adsorption isotherms), environmental fate (*e.g.,* aggregation and dissolution), and biological effects (*e.g.,* uptake, accumulation, and toxicity) of engineered nanomaterials. Future studies are needed to 1) examine the effect of water chemistry (*e.g.,* pH, ionic strength and composition) on NOM corona, and 2) elucidate the interrelationship between the properties of NOM corona and the environmental fate and behavior of NMs and NOM in aquatic environments.

CRediT authorship contribution statement

Dr. Baalousha performed the experimental work, Dr. Sikder synthesized and characterized the platinum nanomaterials, Dr. Poulin extracted and characterized the natural organic matter, Dr. Baalousha, Dr. Tfaily, and Dr. Hess co-analyzed and co-interpreted the FT-ICR-MS data. All authors contributed to the writing and editing of the manuscript.

Declaration of competing interest

The authors declare no conflict of interest.

Acknowledgment

We acknowledge funding from the National Science Foundation (NSF#1738340). All FT-ICR-MS analyses were performed at EMSL, the Environmental Molecular Science Laboratory (grid.436923.9), a DOE Office of Science User Facility sponsored by the Biological and Environmental Research program at the Pacific Northwest National Laboratory.

Appendix A. Supplementary data

Supplementary data to this article can be found online at https://doi.org/10.1016/j.scitotenv.2021.150477.

References

Afshinnia, K., Gibson, I., Merrifield, R., Baalousha, M., 2016. The concentration-dependent aggregation of ag NPs induced by cystine. Sci. Total Environ. 557–558, 395–403.
Afshinnia, K., Sikder, M., Cai, B., Baalousha, M., 2017. Effect of nanomaterial and media physicochemical properties on Ag NM aggregation kinetics. J. Colloid Interface Sci. 487, 192–200.
Aiken, G.R., McKnight, D.M., Thorn, K., Thurman, E., 1992. Isolation of hydrophilic organic acids from water using nonionic macroporous resins. Org. Geochem. 18, 567–573.
Avneri-Katz, S., Young, R.B., McKenna, A.M., Chen, H., Corilo, Y.E., Polubesova, T., et al., 2017. Adsorptive fractionation of dissolved organic matter (DOM) by mineral soil: macroscale approach and molecular insight. Org. Geochem. 103, 113–124.
Baalousha, M., 2009. Aggregation and disaggregation of iron oxide nanoparticles: influence of particle concentration, pH and natural organic matter. Sci. Total Environ. 407, 2093–2101.
Baalousha, M., 2017. Effect of nanomaterial and media physicochemical properties on nanomaterial aggregation kinetics. NanoImpact 6, 55–68.
Baalousha, M., Manciulea, A., Cumberland, S., Kendall, K., Lead, J.R., 2008. Aggregation and surface properties of iron oxide nanoparticles; influence of pH and natural organic matter. Environ. Toxicol. Chem. 27, 1875–1882.
Baalousha, M., Arkill, K.P., Romer, I., Palmer, R.E., Lead, J.R., 2015. Transformations of citrate and tween coated silver nanoparticles reacted with Na2S. Sci. Total Environ. 502, 344–353.
Baalousha, M., Afshinnia, K., Guo, L., 2018. Natural organic matter composition determines the molecular nature of silver nanomaterial-NOM corona. Environ. Sci.: Nano 5, 868–881.
Bocca, B., Petrucci, F., Alimonti, A., Caroli, S., 2003. Traffic-related platinum and rhodium concentrations in the atmosphere of Rome. J. Environ. Monit. 5, 563–568.
Chin, Y.-P., Aiken, G., O'Loughlin, E., 1994. Molecular weight, polydispersity, and spectroscopic properties of aquatic humic substances. Environ. Sci. Technol. 28, 1853–1858.
Claret, F., Schäfer, T., Brevet, J., Reiller, P.E., 2008. Fractionation of Suwannee River fulvic acid and Aldrich humic acid on a-Al2O3: spectroscopic evidence. Environ. Sci. Technol. 42, 8809–8815.
D'Andrilli, J., Dittmar, T., Koch, B.P., Purcell, J.M., Marshall, A.G., Cooper, W.T., 2010. Comprehensive characterization of marine dissolved organic matter by Fourier transform ion cyclotron resonance mass spectrometry with electrospray and atmospheric pressure photoionization. Rapid Commun. Mass Spectrom. 24, 643–650.
Davis, J.A., Gloor, R., 1981. Adsorption of dissolved organics in lake water by aluminum oxide. Effect of molecular weight. Environ. Sci. Technol. 15, 1223–1229.
Deonarine, A., Lau, B.L.T., Aiken, G.R., Ryan, J.N., Hsu-Kim, H., 2011a. Effects of humic substances on precipitation and aggregation of zinc sulfide nanoparticles. Environ. Sci. Technol. 45, 3217–3223.
Deonarine, A., Lau, B.L.T., Aiken, G.R., Ryan, J.N., Hsu-Kim, H., 2011b. Effects of humic substances on precipitation and aggregation of zinc sulfide nanoparticles. Environ. Sci. Technol. 45, 3217–3223.
Diegoli, S., Manciulea, A.L., Begum, S., Jones, I.P., Lead, J.R., Preece, J.A., 2008. Interaction between manufactured gold nanoparticles and naturally occurring organic macromolecules. Sci. Total Environ. 402, 51–61.
Dittmar, T., Koch, B., Hertkorn, N., Kattner, G., 2008. A simple and efficient method for the solid-phase extraction of dissolved organic matter (SPE-DOM) from seawater. Limnol. Oceanogr. Methods 6, 230–235.
Fink, J., Kiely, C.J., Bethell, D., Schiffrin, D.J., 1998. Self-organization of nanosized gold particles. Chem. Mater. 10, 922–926.
Folens, K., Van Acker, T., Bolea-Fernandez, E., Cornelis, G., Vanhaecke, F., Du Laing, G., et al., 2018. Identification of platinum nanoparticles in road dust leachate by single particle inductively coupled plasma-mass spectrometry. Sci. Total Environ. 615, 849–856.
Frost, M.S., Dempsey, M.J., Whitehead, D.E., 2017. The response of citrate functionalised gold and silver nanoparticles to the addition of heavy metal ions. Colloids Surf. A Physicochem. Eng. Asp. 518, 15–24.
Galindo, C., Del Nero, M., 2014. Molecular level description of the sorptive fractionation of a fulvic acid on aluminum oxide using electrospray ionization Fourier transform mass spectrometry. Environ. Sci. Technol. 48, 7401–7408.
Galindo, C., Del Nero, M., 2015. Chemical fractionation of a terrestrial humic acid upon sorption on alumina by high resolution mass spectrometry. RSC Adv. 5, 73058–73067.
Gao, Y., Jiang, P., Liu, D., Yuan, H., Yan, X., Zhou, Z., et al., 2004. Evidence for the monolayer assembly of poly (vinylpyrrolidone) on the surfaces of silver nanowires. J. Phys. Chem. B 108, 12877–12881.
Ghosh, S., Zhen-Yu, W., Kang, S., Bhowmik, P., Xing, B., 2009. Sorption and fractionation of a peat derived humic acid by kaolinite, montmorillonite, and goethite. Pedosphere 19, 21–30.
Ghosh, S., Jiang, W., McClements, J.D., Xing, B., 2011. Colloidal stability of magnetic iron oxide nanoparticles: influence of natural organic matter and synthetic polyelectrolytes. Langmuir 27, 8036–8043.
Gondikas, A.P., Morris, A., Reinsch, B.C., Marinakos, S.M., Lowry, G.V., Hsu-Kim, H., 2012. Cysteine-induced modifications of zero-valent silver nanomaterials: implications for particle surface chemistry, aggregation, dissolution, and silver speciation. Environ. Sci. Technol 46, 7037–7045.
Green, N.W., Perdue, E.M., Aiken, G.R., Butler, K.D., Chen, H., Dittmar, T., et al., 2014. An intercomparison of three methods for the large-scale isolation of oceanic dissolved organic matter. Mar. Chem. 161, 14–19.
Gu, B., Schmitt, J., Chen, Z., Liang, L., McCarthy, J.F., 1994. Adsorption and desorption of natural organic matter on iron oxide: mechanisms and models. Environ. Sci. Pollut. Res. 28, 38–46.
Gunsolus, I.L., Mousavi, M.P., Hussein, K., Bühlmann, P., Haynes, C.L., 2015. Effects of humic and fulvic acids on silver nanoparticle stability, dissolution, and toxicity. Environ. Sci. Technol. 49, 8078–8086.
Henglein, A., 1998. Colloidal silver nanoparticles: photochemical preparation and interaction with O2, CCl4, and some metal ions. Chem. Mater. 10, 444–450.
Hu, P., Chen, L., Kang, X., Chen, S., 2016. Surface functionalization of metal nanoparticles by conjugated metal–ligand interfacial bonds: impacts on intraparticle charge transfer. Acc. Chem. Res. 49, 2251–2260.
Huffman Jr., E., Stuber, H., 1985. Analytical Methodology for Elemental Analysis of Humic Substances.
Hummer, G., Garde, S., Garcia, A.E., Pohorille, A., Pratt, L.R., 1996. An information theory model of hydrophobic interactions. Proc. Natl. Acad. Sci. 93, 8951–8955.
Hur, J., Schlautman, M.A., 2004. Effects of pH and phosphate on the adsorptive fractionation of purified Aldrich humic acid on kaolinite and hematite. J. Colloid Interface Sci. 277, 264–270.

Jiang, C., Castellon, B.T., Matson, C.W., Aiken, G.R., Hsu-Kim, H., 2017. Relative contributions of copper oxide nanoparticles and dissolved copper to cu uptake kinetics of gulf killifish (Fundulus grandis) embryos. Environ. Sci. Technol. 51, 1395–1404.
Kaiser, K., 2003. Sorption of natural organic matter fractions to goethite (α-FeOOH): effect of chemical composition as revealed by liquid-state 13C NMR and wet-chemical analysis. Org. Geochem. 34, 1569–1579.
Kan, C., Cai, W., Li, C., Zhang, L., 2005. Optical studies of polyvinylpyrrolidone reduction effect on free and complex metal ions. J. Mater. Res. 20, 320–324.
Kedia, A., Kumar, P.S., 2012. Solvent-adaptable poly (vinylpyrrolidone) binding induced anisotropic shape control of gold nanostructures. J. Phys. Chem. C 116, 23721–23728.
Khanna, P., Gokhale, R., Subbarao, V., 2004. Poly (vinyl pyrolidone) coated silver nano powder via displacement reaction. J. Mater. Sci. 39, 3773–3776.
Koczkur, K.M., Mourdikoudis, S., Polavarapu, L., Skrabalak, S.E., 2015. Polyvinylpyrrolidone (PVP) in nanoparticle synthesis. Dalton Trans. 44, 17883–17905.
Kteeba, S.M., El-Adawi, H.I., El-Rayis, O.A., El-Ghobashy, A.E., Schuld, J.L., Svoboda, K.R., et al., 2017. Zinc oxide nanoparticle toxicity in embryonic zebrafish: mitigation with different natural organic matter. Environ. Pollut. 230, 1125–1140.
Lau, B.L.T., Hockaday, W.C., Ikuma, K., Furman, O., Decho, A.W., 2013. A preliminary assessment of the interactions between the capping agents of silver nanoparticles and environmental organics. Colloids Surf. A Physicochem. Eng. Asp. 435, 22–27.
Lazaridis, T., Paulaitis, M.E., 1992. Entropy of hydrophobic hydration: a new statistical mechanical formulation. J. Phys. Chem. 96, 3847–3855.
Linlin, Z., Tanaka, K., 2014. Dissolution of silver nanoparticles in presence of natural organic matter. Adv. Mater. Lett. 5, 6–8.
Loosli, F., Le Coustumer, P., Stoll, S., 2013. TiO2 nanoparticles aggregation and disaggregation in presence of alginate and Suwannee River humic acids. pH and concentration effects on nanoparticle stability. Water Res. 47, 6052–6063.
Louie, S.M., Tilton, R.D., Lowry, G.V., 2013. Effects of molecular weight distribution and chemical properties of natural organic matter on gold nanoparticle aggregation. Environ. Sci. Technol 47, 4245–4254.
Louie, S.M., Spielman-Sun, E.R., Small, M.J., Tilton, R.D., Lowry, G.V., 2015. Correlation of the physicochemical properties of natural organic matter samples from different sources to their effects on gold nanoparticle aggregation in monovalent electrolyte. Environ. Sci. Technol 49, 2188–2198.
Lv, J., Zhang, S., Wang, S., Luo, L., Cao, D., Christie, P., 2016. Molecular-scale investigation with ESI-FT-ICR-MS on fractionation of dissolved organic matter induced by adsorption on iron oxyhydroxides. Environ. Sci. Technol 50, 2328–2336.
Meier, M., Namjesnik-Dejanovic, K., Maurice, P.A., Chin, Y.P., Aiken, G.R., 1999. Fractionation of aquatic natural organic matter upon sorption to goethite and kaolinite. Chem. Geol. 157, 275–284.
Mohd Omar, F., Abdul Aziz, H., Stoll, S., 2014. Aggregation and disaggregation of ZnO nanoparticles: influence of pH and adsorption of Suwannee River humic acid. Sci. Total Environ. 468, 195–201.
Morton, O., Puchelt, H., Hernández, E., Lounejeva, E., 2001. Traffic-related platinum group elements (PGE) in soils from Mexico City. J. Geochem. Explor. 72, 223–227.
Mwaanga, P., Carraway, E., Schlautman, M., 2014. Preferential sorption of some natural organic matter fractions to titanium dioxide nanoparticles: influence of pH and ionic strength. Environ. Monit. Assess. 186, 8833–8844.
Nason, J.A., McDowell, S.A., Callahan, T.W., 2012a. Effects of natural organic matter type and concentration on the aggregation of citrate-stabilized gold nanoparticles. J. Environ. Monit. 14, 1885–1892.
Nason, J.A., McDowell, S.A., Callahan, T.W., 2012b. Effects of natural organic matter type and concentration on the aggregation of citrate-stabilized gold nanoparticles. J. Environ. Monit. 14, 1885–1892.
Özkar, S., Finke, R.G., 2002. Nanocluster formation and stabilization fundamental studies: ranking commonly employed anionic stabilizers via the development, then application, of five comparative criteria. J. Am. Chem. Soc. 124, 5796–5810.
Orton, D.J., Tfaily, M.M., Moore, R.J., Lamarche, B.L., Zheng, X., Fillmore, T.L., Chu, R.K., et al., 2018. A customizable flow injection system for automated, high throughput and time sensitive ion mobility spectrometry and mass spectrometry measurements. Anal. Chem. 90 (1), 737–744. https://doi.org/10.1021/acs.analchem.7b02986 PNNL-SA-128111.
Pawlak, J., Łodyga-Chruścińska, E., Chrustowicz, J., 2014. Fate of platinum metals in the environment. J. Trace Elem. Med. Biol. 28, 247–254.
Perera, G.S., Athukorale, S.A., Perez, F., Pittman Jr., C.U., Zhang, D., 2018. Facile displacement of citrate residues from gold nanoparticle surfaces. J. Colloid Interface Sci. 511, 335–343.
Poulin, B.A., Ryan, J.N., Nagy, K.L., Stubbins, A., Dittmar, T., Orem, W., et al., 2017. Spatial dependence of reduced sulfur in Everglades dissolved organic matter controlled by sulfate enrichment. Environ. Sci. Technol. 51, 3630–3639.
Römer, I., Wang, Z.W., Merrifield, R.C., Palmer, R.E., Lead, J., 2016. High resolution STEM-EELS study of silver nanoparticles exposed to light and humic substances. Environ. Sci. Technol. 50, 2183–2190.
Ryu, J.H., Han, S.S., Kim, D.H., Henkelman, G., Lee, H.M., 2011. Ligand-induced structural evolution of Pt55 nanoparticles: amine versus thiol. ACS Nano 5, 8515–8522.
Schäfer, J., Puchelt, H., 1998. Platinum-group-metals (PGM) emitted from automobile catalytic converters and their distribution in roadside soils. J. Geochem. Explor. 64, 307–314.
Sikder, M., Wang, J., Chandler, G.T., Berti, D., Baalousha, M., 2019. Synthesis, characterization, and environmental behaviors of monodispersed platinum nanoparticles. J. Colloid Interface Sci. 540, 330–341.
Sikder, M., Wang, J., Poulin, B.A., Tfaily, M.M., Baalousha, M., 2020. Nanoparticle size and natural organic matter composition determine aggregation behavior of polyvinylpyrrolidone coated platinum nanoparticles. Environ. Sci. Nano 7, 3318–3332.
Song, J.E., Phenrat, T., Marinakos, S., Xiao, Y., Liu, J., Wiesner, M.R., et al., 2011. Hydrophobic interactions increase attachment of gum arabic- and PVP-coated ag nanoparticles to hydrophobic surfaces. Environ. Sci. Technol. 45, 5988–5995.
Tejamaya, M., Romer, I., Merrifield, R.C., Lead, J.R., 2012. Stability of citrate, PVP, and PEG coated silver nanoparticles in ecotoxicology media. Environ. Sci. Technol. 46, 7011–7017.
Tfaily, M.M., Hodgkins, S., Podgorski, D.C., Chanton, J.P., Cooper, W.T., 2012. Comparison of dialysis and solid-phase extraction for isolation and concentration of dissolved organic matter prior to fourier transform ion cyclotron resonance mass spectrometry. Anal. Bioanal. Chem. 404, 447–457.
Tfaily, M.M., Chu, R.K., Tolić, N., Roscioli, K.M., Anderton, C.R., Paša-Tolić, L., et al., 2015. Advanced solvent based methods for molecular characterization of soil organic matter by high-resolution mass spectrometry. Anal. Chem. 87, 5206–5215.
Tolic, N., Liu, Y., Liyu, A.V., Shen, Y., Tfaily, M.M., Kujawinski, E.B., Longnecker, K., et al., 2017. Formularity: software for automated formula assignment of natural and other organic matter from ultra-high resolution mass spectra. Anal. Chem. 89 (23), 12659–12665. https://doi.org/10.1021/acs.analchem.7b03318 PNNL-SA-128094.
Thomas, K.G., Zajicek, J., Kamat, P.V., 2002. Surface binding properties of tetraoctylammonium bromide-capped gold nanoparticles. Langmuir 18, 3722–3727.
Ücer, A., Uyanik, A., Aygün, S.P., 2006. Adsorption of Cu(II), Cd(II), Zn(II), Mn(II) and Fe(III) ions by tannic acid immobilised activated carbon. Sep. Purif. Technol. 47, 113–118.
Wand, P., Bartl, J.D., Heiz, U., Tschurl, M., Cokoja, M., 2016. Functionalization of small platinum nanoparticles with amines and phosphines: ligand binding modes and particle stability. J. Colloid Interface Sci. 478, 72–80.
Weishaar, J.L., Aiken, G.R., Bergamaschi, B.A., Fram, M.S., Fujii, R., Mopper, K., 2003. Evaluation of specific ultraviolet absorbance as an indicator of the chemical composition and reactivity of dissolved organic carbon. Environ. Sci. Technol 37, 4702–4708.
Yang, S.P., Bar-Ilan, O., Peterson, R.E., Heideman, W., Hamers, R.J., Pedersen, J.A., 2013. Influence of humic acid on titanium dioxide nanoparticle toxicity to developing zebrafish. Environ. Sci. Technol 47, 4718–4725.
Zhang, J., Liu, H., Wang, Z., Ming, N., 2008. Au-induced polyvinylpyrrolidone aggregates with bound water for the highly shape-selective synthesis of silica nanostructures. Chem. Eur. J. 14, 4374–4380.
Zhang, Y., Xia, J., Liu, Y., Qiang, L., Zhu, L., 2016. Impacts of morphology, natural organic matter, cations, and ionic strength on sulfidation of silver nanowires. Environ. Sci. Technol. 50, 13283–13290.
Zhou, Q., Maurice, P.A., Cabaniss, S.E., 2001. Size fractionation upon adsorption of fulvic acid on goethite: equilibrium and kinetic studies. Geochim. Cosmochim. Acta 65, 803–812.